Progress In Electromagnetics Research B, Vol. 7, 265–280, 2008

A CWA-BASED DETECTION PROCEDURE OF A PERFECTLY-CONDUCTING CYLINDER BURIED IN A DIELECTRIC HALF-SPACE

F. Frezza

Department of Electronic Engineering
"La Sapienza" University of Rome
Via Eudossiana 18, 00184 Roma, Italy

P. Martinelli, L. Pajewski, and G. Schettini

Department of Applied Electronics
"Roma Tre" University
Via della Vasca Navale 84, 00146 Roma, Italy

Abstract—The electromagnetic scattering problem of a short-pulse plane wave by a perfectly-conducting circular cylinder, buried in a dielectric half-space, is solved by means of a cylindrical-wave approach (CWA). The incident plane wave may have a rather general shape in the time domain. The technique is applicable for arbitrary polarization, for any cylinder size and burial depth, and it gives results both in the near- and in the far-field regions. In this work, an application of the technique to a basic but practical detection problem is presented, showing good results.

1. INTRODUCTION

The two-dimensional electromagnetic scattering problem by buried circular cylinders has been discussed by many authors, both from a theoretical and a numerical point of view, due to its application to remote sensing of the earth's subsurface, to the detection of landmines, pipes, conduits, or to communication through the earth [1–6].

An effective tool for the detection and identification of buried objects, with civilian and military applications, is Ground Penetrating Radar (GPR) [7–9]. It uses electromagnetic-wave propagation and scattering to image, locate and quantitatively identify changes in electrical and magnetic properties in the ground. It has

the highest resolution in subsurface imaging in comparison to any geophysical method, approaching centimeters under the right conditions. Depending on material properties, the depth of investigation varies from less than a meter to several meters. Processing and interpretation acquired GPR data, it is possible to extract information such as depth, orientation, size and shape of buried objects, density and water content of soils, and much more [10–13]. The frequencies used in the applications above are chosen to achieve good ground penetration, which necessitates relatively low operating frequencies for typical soils ($< 1\,\mathrm{GHz}$). The bandwidth has to be as large as possible to obtain sufficient temporal and spatial resolution. For these reasons, ultrawideband short-pulse systems are commonly employed: many of them operate in the time domain and have an instantaneous frequency spectrum of approximately 0.1–1.0 GHz [7].

In [6], the plane-wave scattering problem by a finite set of perfectly-conducting cylinders buried in a dielectric half-space was considered. We developed a Cylindrical-Wave Approach (CWA), in which the field scattered by the cylinders is decomposed in cylindrical waves. The reflection and transmission properties of such waves in the presence of plane interfaces have been discussed in [14] and [15], by introducing suitable reflected and transmitted cylindrical functions and the relevant spectral integrals. Such integrals have been numerically solved employing suitable adaptive integration techniques of Gaussian type, together with convergence-acceleration algorithms [16, 17]. Our spectral-domain method may deal with both TM and TE polarization cases, and yields results in both the near- and the far-field zones. All the multiple reflections between the cylinders and the interface are taken into account. It is noted that the CWA can be employed to characterize two-dimensional obstacles of arbitrary shape simulated by a suitable array of circular cylinders [6, 18].

In [2], the method was extended to study the scattering, from buried perfectly-conducting cylinders, of a pulsed plane wave with a rather general time-shape. To solve such time-domain problem, we performed a sampling of the incident-field spectrum, we worked out the solution for any sample in the frequency domain by using the CWA, and we calculated the solution in the time domain by means of the inverse transform.

In this paper, attention is paid to an application of the technique presented in [2] to a practical, basic, detection problem. The curves of the field, scattered by a buried cylinder and transmitted back to the air, can be interpreted as if they were plotted from GPR data acquired in an unknown scenario, in order to extract geometrical information about the buried object, as for example its depth and size.

2. THE SCATTERING PROBLEM

The geometry of the scattering problem is shown in Fig. 1: a perfectly-conducting circular cylinders is buried in a linear isotropic homogeneous dielectric lossless half-space (medium 1, with permittivity $\varepsilon_1 = \varepsilon_0\varepsilon_{r1} = \varepsilon_0 n_1^2$, where n_1 is the refractive index). The cylinder is parallel to the y axis and is assumed to be infinite along y direction, therefore the problem is two-dimensional.

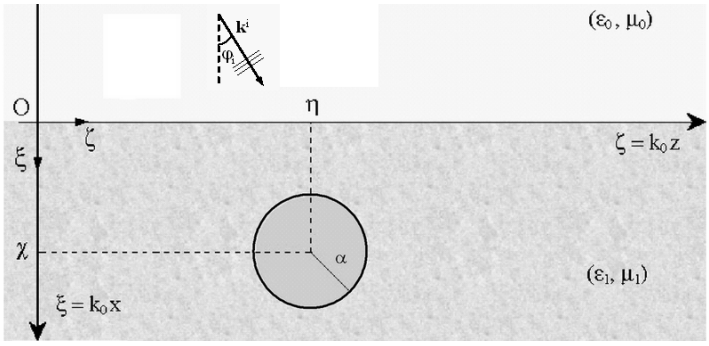

Figure 1. Geometry of the scattering problem.

A pulsed plane wave, with y-directed electric/magnetic field $g(\tau;\mathbf{r})$ (for $\mathrm{TM}^{(y)}/\mathrm{TE}^{(y)}$ polarization, respectively) , has a propagation direction lying in the xz plane and impinges at an angle φ_i from medium 0 (a vacuum) on the planar interface with medium 1. The time variable $\tau = \omega_0 t$ is normalized with respect to $\omega_0 = k_0 c_0$, where k_0 is the vacuum wavenumber, and c_0 is the light velocity in a vacuum; moreover, $\mathbf{r} = (x, z)$.

We introduce a reference frame (O, ξ, ζ), with normalized frequency-depending coordinates $\xi = k_0 x$ and $\zeta = k_0 z$; $\boldsymbol{\rho} = (\xi, \zeta) = k_0\mathbf{r}$. The cylinder, with normalized radius $\alpha = k_0 a$, has axis located in (χ, η), with $\chi = k_0 h$ and $\eta = k_0 d$.

The function $g(\tau;\boldsymbol{\rho})$ can be expressed as

$$g(\tau;\boldsymbol{\rho}) = \frac{\omega_0}{4\pi^2}\int_{-\infty}^{+\infty}\int_{-\infty}^{+\infty}\gamma\left(\psi,\xi,n_{\|}\right)e^{i\left(n_{\|}\zeta-\psi\tau\right)}d\psi dn_{\|} \tag{1}$$

where $\gamma(\psi,\xi,n_{\|}) = G^{+}(\psi,n_{\|})e^{i\xi(\psi^2-n_{\|}^2)^{\frac{1}{2}}} + G^{-}(\psi,n_{\|})e^{-i\xi(\psi^2-n_{\|}^2)^{\frac{1}{2}}}$ is the Fourier transform along τ and ζ of $g(\tau;\boldsymbol{\rho})$; moreover, $\psi = \omega/\omega_0 = k/k_0$, being ω the angular frequency and k the wavenumber. The pulse $g(\tau;\boldsymbol{\rho})$ propagates from infinite to the planar interface, then it

has to be $G^{-}\left(\psi, n_{\parallel}\right) \equiv 0$. Since we consider a single plane wave, $G^{+}\left(\psi, n_{\parallel}\right) = 2\pi G\left(\psi\right)\delta\left(n_{\parallel} - \psi\sin\varphi_{\mathrm{i}}\right)$. Therefore

$$g\left(\tau;\boldsymbol{\rho}\right) = \frac{\omega_o}{2\pi}\int_{-\infty}^{+\infty} G\left(\psi\right) e^{i\psi(\xi\cos\varphi_{\mathrm{i}}+\zeta\sin\varphi_{\mathrm{i}}-\tau)} d\psi \tag{2}$$

with $\mathbf{n}^{\mathrm{i}} = (\cos\varphi_{\mathrm{i}}, \sin\varphi_{\mathrm{i}})$, and $g\left(\tau;\boldsymbol{\rho}\right) = g\left(\tau - \mathbf{n}^{\mathrm{i}}\cdot\boldsymbol{\rho}\right)$.

In this paper, we assume that

$$g(\tau;\boldsymbol{\rho}) = g\left(\tau - \mathbf{n}\cdot\boldsymbol{\rho}\right) = g_0 e^{-\frac{(\tau-\mathbf{n}\cdot\boldsymbol{\rho})}{2}}\left[e^{\frac{1}{2}}\cos\left(\tau - \mathbf{n}\cdot\boldsymbol{\rho}\right) - 1\right] \tag{3}$$

where $\mathbf{n} = n_{\perp}\hat{\boldsymbol{\xi}} + n_{\parallel}\hat{\boldsymbol{\zeta}}$ is the unit vector parallel to the wavevector $\mathbf{k}$ of the incident plane wave, and g_0 is an amplitude coefficient. It is plotted in Fig. 2(a), as a function of τ, when $\mathbf{n}\cdot\boldsymbol{\rho} = 0$. Its maximum value is obviously for $\tau = 0$ and is $g_{\mathrm{MAX}} = g_0(e^{\frac{1}{2}} - 1) \cong 0.6487 g_0$. In $\tau = 4$, $g(4) \cong -6\times10^{-4} g(0)$, that is, $|g(4)| < 0.01 g_{\mathrm{MAX}}$. Since $|g(\tau)|$ decreases as τ increases, we can consider approximately the short pulse as of finite duration, vanishing for $\tau \geq \Delta\tau$ with $\Delta\tau = 4$. This waveform is consistent with many pulsed current sources [19–21].

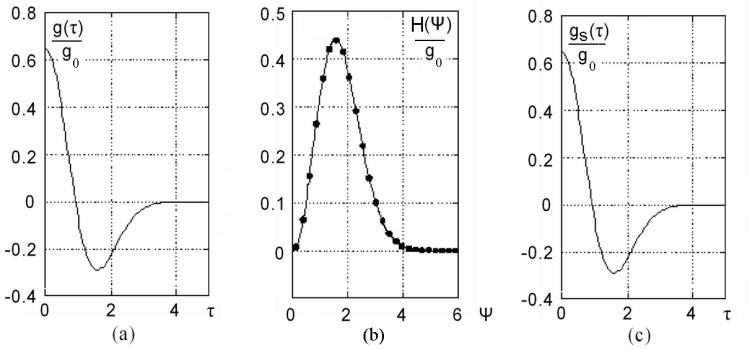

Figure 2. Incident time-domain short pulse used in the numerical calculation (a) and its spectrum (b). (c) Reconstruction of the incident pulse by means of 2440 spectrum samples (the dots reported in (b)), as a function of τ.

The analytical expression of the incident-field spectrum is given by

$$H(\psi,\boldsymbol{\rho}) = G\left(\psi\right) e^{i\psi(\xi\cos\varphi_{\mathrm{i}}+\zeta\sin\varphi_{\mathrm{i}})} = g_0\frac{\sqrt{2\pi}}{\omega_0} e^{-\frac{\psi^2}{2}}\left[\cosh\left(\psi\right) - 1\right] e^{i\psi\mathbf{n}^{\mathrm{i}}\cdot\boldsymbol{\rho}} \tag{4}$$

It is plotted in Fig. 2(b), as a function of ψ, when $\mathbf{n}^{\mathrm{i}}\cdot\boldsymbol{\rho}=0$; its maximum value $G_{\mathrm{MAX}}\cong 1.32\times 10^{9}\ g_0\ \omega_0^{-1}$ is in $\psi\cong 1.5411$ ($\omega\cong 1.5411\omega_0$). In $\psi=6$, $G(6)\cong 9.18\times 10^{3}\ g_0\ \omega_0^{-1}$, i.e., $G(6)<7\times 10^{-6}G_{\mathrm{MAX}}$: then, we can say that the spectrum does not contain normalized frequencies greater than $\psi\geq\Delta\psi$ with $\Delta\psi=6$.

Since the time duration of the pulse is finite, its spectrum can be reconstructed by means of the sampling theorem [22]:

$$H_s(\psi,\boldsymbol{\rho})=\omega_0\Delta\psi_s\sum_{p=-\infty}^{+\infty}H(p\Delta\psi_s,\boldsymbol{\rho}\,)\,\delta(\psi-p\Delta\psi_s) \tag{5}$$

where $\Delta\psi_s$ is the constant frequency pitch.

In order to avoid aliasing phenomena and to recover all the information contained in the continuous spectrum from the sampled one, the well-known Nyquist condition has to be satisfied: $\Delta\psi_s\leq\frac{1}{2\Delta\tau}$, being $2\Delta\tau$ the time duration of the incident pulse. Since $\Delta\tau=4$, it has to be $\Delta\psi_s\leq\frac{1}{8}$. Then, being the bandwidth of our signal spectrum limited to $2\Delta\psi=12$, the number of samples can be finite and, in particular, equal to $\left\lfloor\frac{12}{\Delta\psi_s}\right\rfloor+1$. The sampled spectrum can be rewritten as

$$\begin{aligned}H_s(\psi,\boldsymbol{\rho})&=g_0\Delta\psi_s\sqrt{2\pi}\\&\times\sum_{p=-\left[\frac{6}{\Delta\psi_s}\right]}^{\left[\frac{6}{\Delta\psi_s}\right]}\left\{\frac{e^{\frac{1}{2}}}{2}\left[e^{-\frac{1}{2}(p\Delta\psi_s-1)^2}+e^{-\frac{1}{2}(p\Delta\psi_s+1)^2}\right]-e^{-\frac{p^2(\Delta\psi_s)^2}{2}}\right\}\\&\times e^{ip\Delta\psi_s\mathbf{n}^{\mathrm{i}}\cdot\boldsymbol{\rho}}\delta(\psi-p\Delta\psi_s)\end{aligned} \tag{6}$$

The inverse Fourier transform of (6) is given by

$$\begin{aligned}g_s\left(\tau-\mathbf{n}^{\mathrm{i}}\cdot\boldsymbol{\rho}\right)&=\frac{g_0\Delta\psi_s}{\sqrt{2\pi}}\\&\times\sum_{p=1}^{\left[\frac{6}{\Delta\psi_s}\right]}\left\{\frac{e^{\frac{1}{2}}}{2}\left[e^{-\frac{1}{2}(p\Delta\psi_s-1)^2}+e^{-\frac{1}{2}(p\Delta\psi_s+1)^2}\right]-e^{-\frac{p^2(\Delta\psi_s)^2}{2}}\right\}\\&\times\cos\left(p\Delta\psi_s\mathbf{n}^{\mathrm{i}}\cdot\boldsymbol{\rho}-p\Delta\psi_s\tau\right)\end{aligned} \tag{7}$$

with period $\frac{2\pi}{2\Delta\psi_s}$, that is a superposition of replicas of the incident field separated by $\frac{\pi}{\Delta\psi_s}-8$.

In Fig. 2(b), the samples of the incident spectrum are represented by dots; in Fig. 2(c), the reconstruction of the incident pulse by means

of 2440 spectrum samples is reported. The approximation reveals to be good, the relative error is $\leq 10^{-4}$.

The solution of the scattering problem is carried out in the spectral domain by using the full-wave CWA presented in [6]. The above-described sampling procedure is applied also to the spectra of the various field terms involved: the fields reflected and transmitted by the planar interface, the field scattered by the cylinder, and the fields scattered-reflected and scattered-transmitted by the planar interface. By means of an inverse transform, the solution in the time domain is finally calculated. This procedure is described in detail in [2].

3. A DETECTION PROCEDURE

In this Section we apply the technique presented in [2] to a practical, although basic, detection problem. In particular, we outline a procedure to single out the position and radius of a perfectly-conducting circular cylinder buried in a soil of known refractive index. An observation point $(\xi_{\text{op}}, \zeta_{\text{op}})$ is fixed in medium 0 and close to the interface, the time origin is chosen as coincident with the incident-pulse first maximum in such point.

We concentrate on the early-time response of the structure: we consider the field scattered by the cylinder and transmitted back to the air V_{st} [2] over a time interval which is of the order of the incident-pulse duration, and its propagation from the observation point to the target. The transient regime is very useful for detection, because it contains the bulk of the scattered energy and the information about location and size of buried objects.

The first step of the procedure consists in shifting the observation point along a straight line parallel to the planar interface between air and soil: from the corresponding set of $V_{\text{st}}(t)$ curves, it is possible to determine η. A typical example is given in Fig. 3: each curve of the set corresponds to a particular value of ζ_{op}, and the vertical-axis scale is not significant since a vertical translation is performed, as is customary in GPR output [23]. The delay time of the response is minimum when the observation point lies on the $\zeta_{\text{op}} = \eta$ straight line (i.e., it is aligned with the cylinder center).

In the following, the observation point is always placed aligned with the already-detected cylinder center.

In the second step of the procedure, the instant on which the higher peak in a $|V_{\text{st}}|$ curve is centered can be used to calculate the quantity $\frac{\chi}{k_0} - a$. We found out in our simulations that such $t = t_0$ value corresponds to the absolute minimum of V_{st} for $\text{TM}^{(y)}$ polarization, to the absolute maximum in the $\text{TE}^{(y)}$ case. We have found and tested

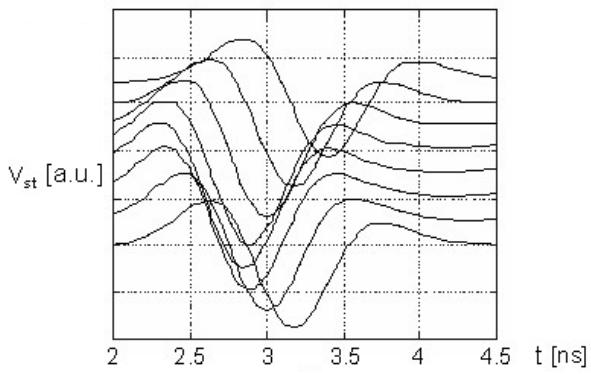

Figure 3. Typical sets of $V_{\rm st}(t)$ curves, as the observation point is translated along ζ, useful for target detection. The vertical-axis scale is not significant.

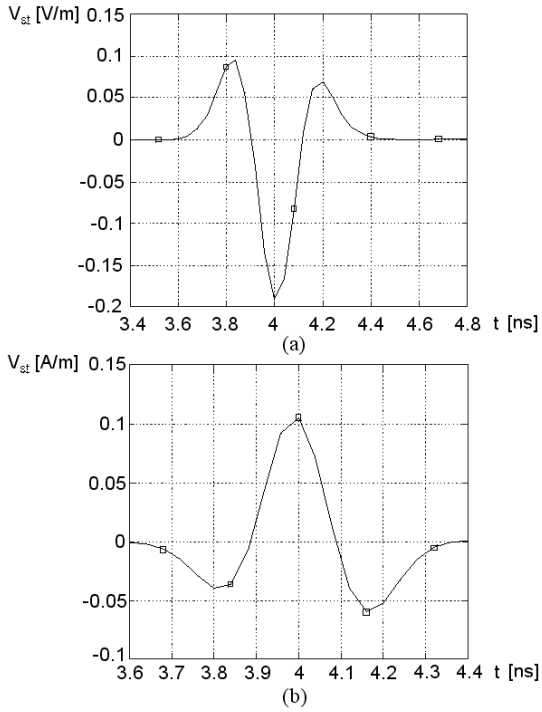

Figure 4. (a) $V_{\rm st}$ vs. t when $-\frac{\mathbf{n}\cdot\mathbf{r}}{c_0} = 1\,\text{ns}$, $n_1 = 1.5$, $a = 2\,\text{cm}$, $\eta = 0$, $k_0 = 30\,\text{m}^{-1}$, $\chi = 0.32k_0$ and the polarization is $\text{TM}^{(y)}$. (b) Same as in (a), when $\chi = 0.35k_0$ and for $\text{TE}^{(y)}$ polarization.

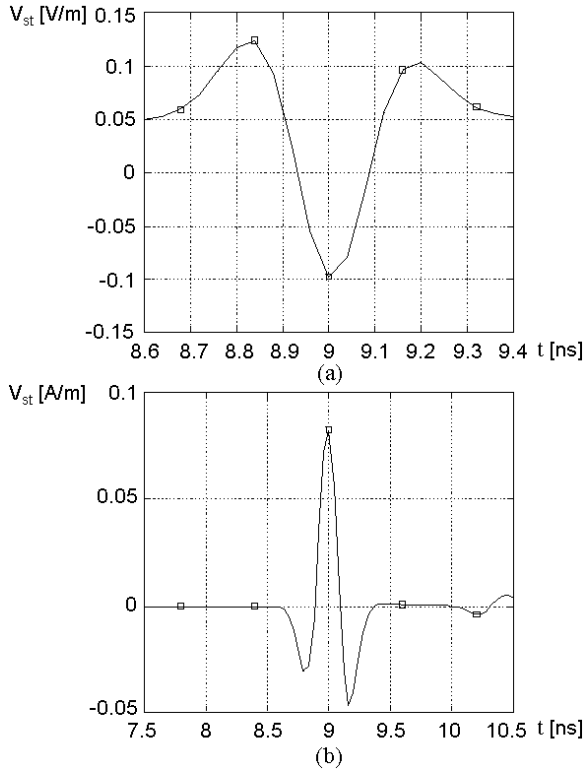

Figure 5. (a) Same as in Fig. 4(a) when $\chi = 0.82k_0$. (b) Same as in Fig. 4(b), when $\chi = 0.85k_0$.

the following rule for cylinder radii greater than 2 cm and time lengths of the incident pulse shorter than 0.9 ns:

$$t_0 = -\frac{\mathbf{n}\cdot\mathbf{r}}{c_0} + \frac{2\left(\dfrac{\chi}{k_0} - a\right)n_1}{c_0} \tag{8}$$

It represents the time interval between the maxima of incident and backscattered field: it corresponds to the propagation time along the vertical path from the observation point to the nearest point of the target and back to the observation point. Two examples are given in Figs. 4 and 5. In these figures, V_{st} is plotted versus t when $n_1 = 1.5$, $a = 2\,\mathrm{cm}$, $\eta = 0$, $k_0 = 30\,\mathrm{m}^{-1}$, $-\frac{\mathbf{n}\cdot\mathbf{r}}{c_0} = 1\,\mathrm{ns}$: in Fig. 4(a) $\chi = 0.32k_0$, and the polarization is $\mathrm{TM}^{(y)}$, in (b) $\chi = 0.35k_0$ and the polarization is $\mathrm{TE}^{(y)}$; in Fig. 5(a) $\chi = 0.82k_0$ and the polarization is $\mathrm{TM}^{(y)}$, in (b)

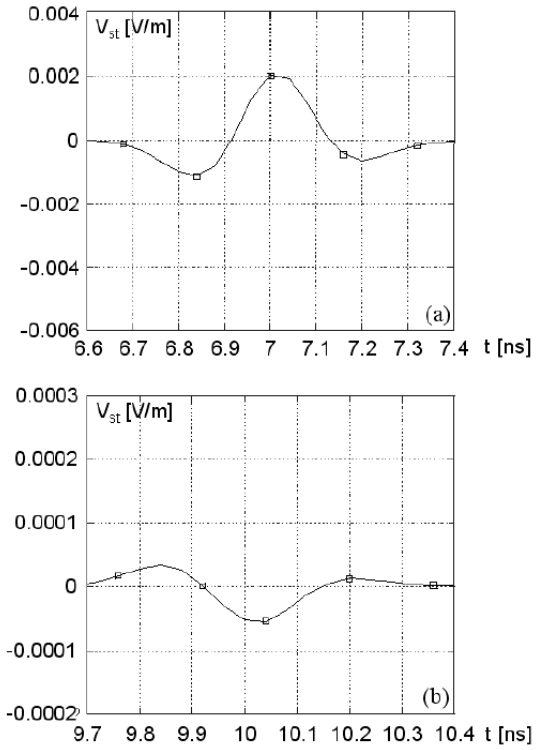

Figure 6. V_{st} vs. t for the same case as in Fig. 4(a): (a) second reflection, (b) third reflection.

$\chi = 0.85k_0$ and the polarization is $\mathrm{TE}^{(y)}$. It can be appreciated that t_0 always verifies Eq. (8) rule.

It is worth stressing that the first absolute $|V_{\mathrm{st}}|$ maximum is, in both polarization cases, followed by local maxima in $t = t_{0\mathrm{m}}$ $(m = 1, 2, 3, \ldots)$:

$$t_{0\mathrm{m}} = -\frac{\mathbf{n} \cdot \mathbf{r}}{c_0} + \frac{2\mathrm{m}\left(\dfrac{\chi}{k_0} - a\right) n_1}{c_0} \tag{9}$$

Such weaker peaks correspond to multiple reflections between the buried cylinder and the planar air-soil interface. Note that the first return, as well as the following echoes, somehow resemble in shape the incident pulse (eventually with the sign changed). Figures 6 and 7 show the peaks relevant to the second (graph (a)) and third (graph

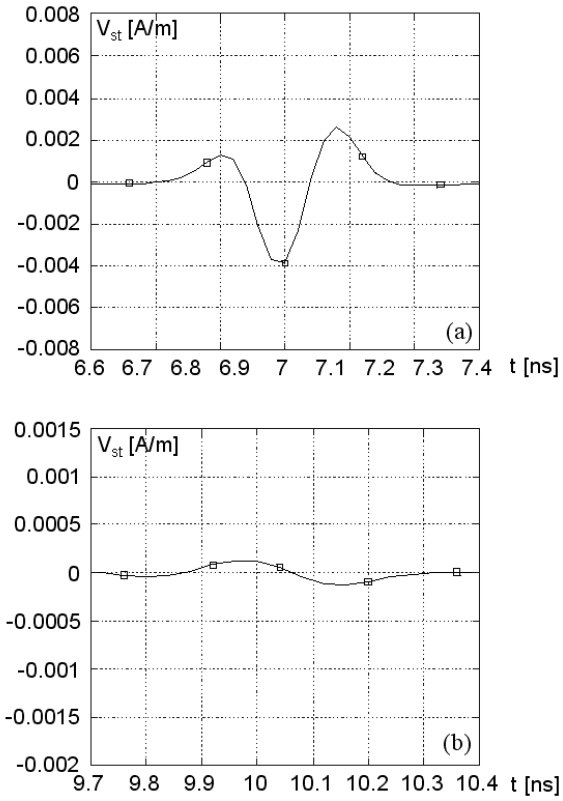

Figure 7. $V_{\rm st}$ vs. t for the same case as in Fig. 4(b): (a) second reflection, (b) third reflection.

(b)) reflections in $\mathrm{TM}^{(y)}$ and $\mathrm{TE}^{(y)}$ polarization, respectively, for the same cases as in Figs. 4(a) and 4(b). Of course, at each reflection the back-scattered field amplitude decreases.

The third step in our detection procedure is the determination of the target radius. Obviously, once a is obtained, it is possible to calculate χ directly from the second-step results. In Fig. 8 different values of a are considered, while keeping fixed the difference $\frac{\chi}{k_0} - a$: in particular, in Fig. 8(a) $V_{\rm st}$ is shown as a function of t when $k_0 = 30\,\mathrm{m}^{-1}$, for $\mathrm{TM}^{(y)}$ polarization, $\frac{\chi}{k_0} - a = 50$ cm: $a = 3$, 6, or 9 cm; in Fig. 8(b), the same as in (a) is reported for $\mathrm{TE}^{(y)}$ polarization, $\frac{\chi}{k_0} - a = 30$ cm: $a = 2$, 4, or 5 cm. Figure 9 is an extension of Fig. 8. From the graphs reported in Fig. 8, it can be appreciated that the peaks examined in the previous step of our procedure, due to the reverberations between

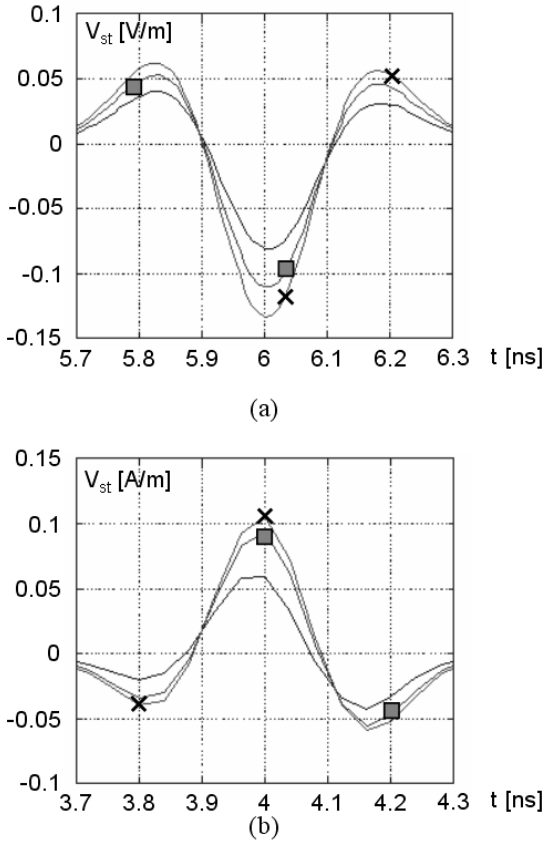

Figure 8. (a) $V_{\rm st}$ as a function of t when $k_0 = 30\,{\rm m}^{-1}$, for TM$^{(y)}$ polarization, $\frac{\chi}{k_0} - a = 50\,{\rm cm}$: $a = 3\,{\rm cm}$ (full line), $a = 6\,{\rm cm}$ (full line with squares), or $a = 9$ cm (full line with crosses). (b) Same as in (a) for TE$^{(y)}$ polarization, $\frac{\chi}{k_0} - a = 30\,{\rm cm}$: $a = 2\,{\rm cm}$ (full line), $a = 4\,{\rm cm}$ (full line with squares), or $a = 5\,{\rm cm}$ (full line with crosses).

the target and the air-soil interface, are centered on fixed instants, as they depend on the quantity $\frac{\chi}{k_0} - a$. The graphs of Fig. 9 show, however, that in the $V_{\rm st}$ curve other peaks are present: they are not simultaneous and shift towards larger values of t as a becomes larger. We have conjectured that such peaks could be generated by to the so-called *creeping wave* [24], guided by the curved surface of the cylinder: in other words, they are connected to the signal propagation along the vertical path from the observation point to the target,

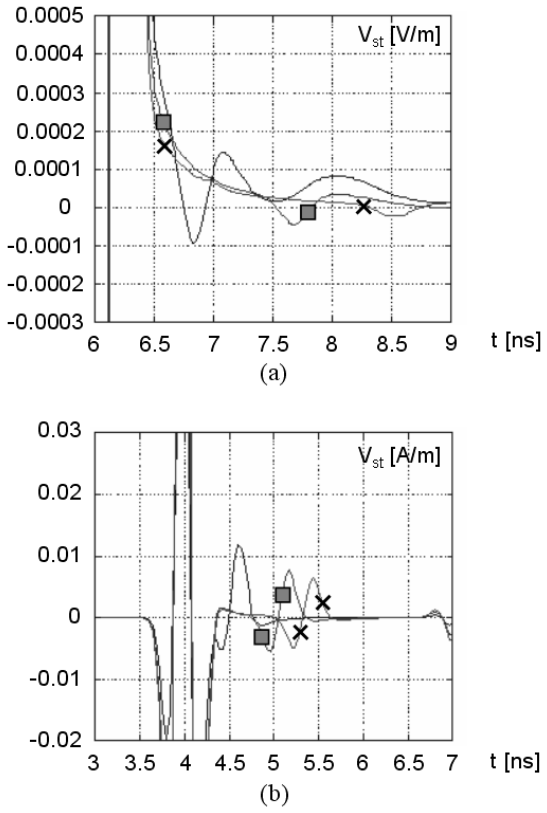

Figure 9. Extensions of the plots reported in Fig. 8.

circumnavigation of the cylinder at a velocity slower than the light one, and coming back to the observation point.

If $t_{\rm cw}$ is the instant of the maximum (or minimum) in the creeping-wave peak, we estimated and plotted the quantity $|t_{\rm cw}-t_0|$ as a function of a: we found that such time interval is proportional to the cylinder radius (see Figs. 10(a) and (b)), with a proportionality constant independent of other involved physical and geometrical parameters, such as the incident pulse duration (Figs. 10(c) and (d)), or the quantity $\frac{\chi}{k_0} - a$ (Figs. 10(e) and (f)). Therefore, from the knowledge of $V_{\rm st}(t)$ it is possible to extract, through $t_{\rm cw}$, the size of the buried object.

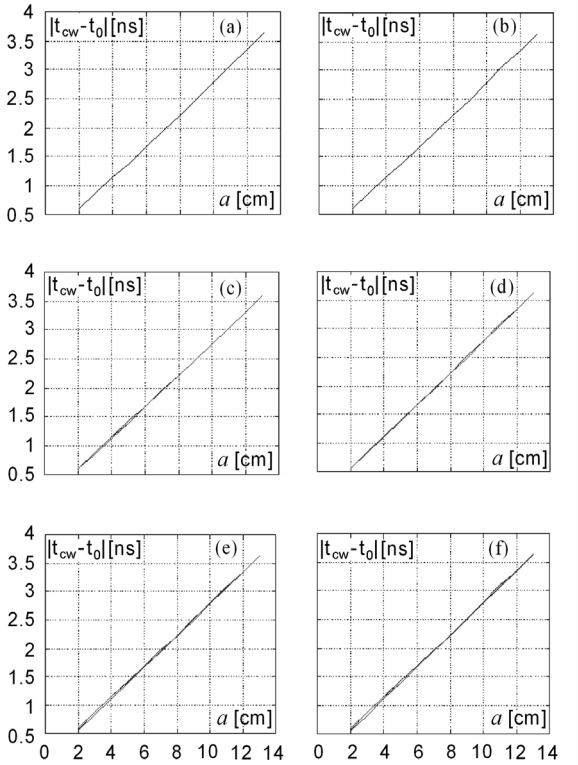

Figure 10. (a) Time interval $|t_{\rm cw} - t_0|$ as a function of a, when $k_0 = 30\,\mathrm{m}^{-1}$, $\mathrm{TM}^{(y)}$ polarization, $\frac{\chi}{k_0} - a = 1\,\mathrm{m}$. (b) Same as in (a) for $\mathrm{TE}^{(y)}$ polarization. (c) and (d) Same as in (a) and (b), sets of curves with k_0 ranging from 30 to $50\,\mathrm{m}^{-1}$. (e) and (f) Same as in (a) and (b), sets of curves with $\frac{\chi}{k_0} - a$ ranging from 0.5 m to 1 m.

4. CONCLUSIONS

We have presented an analytic solution for the electromagnetic scattering problem of a short-pulse plane wave by a finite set of buried perfectly-conducting circular cylinders. The method has been applied to both TE and TM polarizations. For the simpler case of one buried cylinder, we investigated the effects of the various geometrical parameters involved: cylinder position and radius, position of the observation point, incident-pulse time duration. Finally, the technique has been applied to the practical case of the detection of one buried perfectly-conducting cylinder, yielding good results for the depth and

the size of the buried object.

Future work is in progress, for the detection of a set of cylinders and the extension to dielectric objects. Moreover, since the scattering algorithm is implemented in the frequency domain, it may be employed to model dispersive soils.

REFERENCES

1. Van den Bosch, I., S. Lambot, M. Acheroy, I. Huynen, and P. Druyts, "Accurate and efficient modeling of monostatic GPR signal of dielectric targets buried in stratified media," *Journal of Electromagnetic Waves and Applications*, Vol. 20, No. 3, 283–290, 2006.
2. Frezza, F., P. Martinelli, L. Pajewski, and G. Schettini, "Short-pulse electromagnetic scattering from buried perfectly-conducting cylinders," *IEEE Letters on Geoscience and Remote Sensing*, Vol. 4, No. 4, 611–615, Oct. 2007.
3. Chen, H. T. and G.-Q. Zhu, "Model the electromagnetic scattering from three-dimensional PEC object buried under rough ground by MOM and modified PO hybrid method," *Progress In Electromagnetics Research*, PIER 77, 15–27, 2007.
4. Li, Z.-X., "Bistatic scattering from rough dielectric soil surface with a conducting object with arbitrary closed contour partially buried by using the FBM/SAA method," *Progress In Electromagnetics Research*, PIER 76, 253–274, 2007.
5. Ahmed, S. and Q. A. Naqvi, "Electromagnetic scattering from a perfect electromagnetic conductor cylinder buried in a dielectric half-space," *Progress In Electromagnetics Research*, PIER 78, 25–38, 2008.
6. Di Vico, M., F. Frezza, L. Pajewski, and G. Schettini, "Scattering by a finite set of perfectly conducting cylinders buried in a dielectric half-space: A spectral-domain solution," *IEEE Trans. Antennas Propagat.*, Vol. 53, 719–727, Feb. 2005.
7. Daniels, D. J., *Surface-Penetrating Radar*, 2nd edition, IEE Radar Series, London, 2004.
8. Uduwawala, D., "Modeling and investigation of planar parabolic dipoles for GPR applications: a comparison with bow-tie using FDTD," *Journal of Electromagnetic Waves and Applications*, Vol. 20, No. 2, 227–236, 2006.
9. Moustafa, K. and K. A. Hussein, "Performance evaluation of separated aperture sensor GPR system for land mine detection," *Progress In Electromagnetics Research*, PIER 72, 21–37, 2007.

10. Chen, X., K. Huang, and X.-B. Xu, "Microwave imaging of buried inhomogeneous objects using parallel genetic algorithm combined with FDTD method," *Progress In Electromagnetics Research*, PIER 53, 283–298, 2005.
11. Nishimoto, M., S. Ueno, and Y. Kimura, "Feature extraction from GPR data for identification of landmine-like objects under rough ground surface," *Journal of Electromagnetic Waves and Applications*, Vol. 20, No. 12, 1577–1586, 2006.
12. Thomas, V., J. Yohannan, A. Lonappan, G. Bindu, and K. T. Mathew, "Localization of the investigation domain in electromagnetic imaging of buried 2-D dielectric pipelines with circular cross section," *Progress In Electromagnetics Research*, PIER 61, 111–131, 2006.
13. Tiwari, K. C., D. Singh, and M. K. Arora, "Development of a model for detection and estimation of depth of shallow buried non-metallic landmine at microwave X-band frequency," *Progress In Electromagnetics Research*, PIER 79, 225–250, 2008.
14. Borghi, R., F. Gori, M. Santarsiero, F. Frezza, and G. Schettini, "Plane-wave scattering by a perfectly conducting circular cylinder near a plane surface: cylindrical-wave approach," *J. Opt. Soc. Am. A*, Vol. 13, 483–493, Mar. 1996.
15. Ciambra, F., F. Frezza, L. Pajewski, and G. Schettini, "A spectral-domain solution for the scattering problem of a circular cylinder buried in a dielectric half-space," *Progress In Electromagnetics Research*, PIER 38, 223–252, 2002.
16. Borghi, R., F. Frezza, M. Santarsiero, C. Santini, and G. Schettini, "Numerical study of the reflection of cylindrical waves of arbitrary order by a generic planar interface," *J. of Electromagnetic Waves and Appl.*, Vol. 13, 27–50, Jan. 1999.
17. Borghi, R., F. Frezza, M. Santarsiero, C. Santini, and G. Schettini, "A quadrature algorithm for the evaluation of a 2D radiation integral with highly oscillating kernel," *J. of Electromagnetic Waves and Appl.*, Vol. 14, 1353–1370, Oct. 2000.
18. Di Vico, M., F. Frezza, L. Pajewski, and G. Schettini, "Scattering by buried dielectric cylindrical structures," *Radio Science*, Vol. 40, No. 6, RS6S18, Aug. 2005.
19. Bertoni, H. L., L. Carin, and L. B. Felsen (eds.), *Ultra-Wideband, Short-Pulse Electromagnetics*, Plenum, New York, 1994.
20. Carin, L. and L. B. Felsen (eds.), *Ultra-Wideband, Short-Pulse Electromagnetics II*, Plenum, New York, 1995.
21. Losada, V., R. R. Boix, and F. Medina, "Short-pulse

electromagnetic scattering from conducting circular plates," *IEEE Trans. Geosci. Remote Sensing*, Vol. 41, 987–997, May 2003.

22. Brigham, E. O., *The Fast Fourier Transform and Its Applications*, Prentice-Hall, New Jersey, 1988.
23. Gürel, L. and U. Oğuz, "Three-dimensional FDTD modeling of a ground-penetrating radar," *IEEE Trans. Geosci. Remote Sensing*, Vol. 38, No. 4 1513–1521, 2000.
24. Felsen, L. B. and N. Marcuvitz, *Radiation and Scattering of Waves*, IEEE Press, New York, 1994.